Supplementary materials: Dimensional Crossover of Microscopic Magnetic Metasurfaces for Magnetic Field Amplification

N. Lejeune,[1] E. Fourneau,[1] A. Barrera,[2] O. Morris,[3] O. Leonard,[3] J. A. Arregi,[4] C. Navau,[5] V. Uhlíř,[4,6] S. Bending,[3] A. Palau,[2] and A. V. Silhanek[1]

[1)] *Experimental Physics of Nanostructured Materials, Department of Physics, Université de Liège, B-4000 Sart Tilman, Belgium.*

[2)] *Insititut de Ciència de Materials de Barcelona, ICMAB-CSIC, Campus de la UAB 08193 Bellaterra, Spain.*

[3)] *Centre for Nanoscience and Nanotechnology, Department of Physics, University of Bath, Bath, BA2 7AY, United Kingdom.*

[4)] *CEITEC BUT, Brno University of Technology, Purkyňova 123, 612 00 Brno, Czech Republic.*

[5)] *Grup d'Electromagnetisme, Departament de Fisica, Universitat Autonoma de Barcelona, 08193 Bellaterra, Barcelona, Spain.*

[6)] *Institute of Physical Engineering, Brno University of Technology, Technická 2, 616 69 Brno, Czechia.*

(*Corresponding author: asilhanek@uliege.be)

(*Corresponding author: palau@icmab.es)

(Dated: 9 July 2024)

I. MAGNETO-OPTICAL KERR MICROSCOPY ANALYSIS

MOKE microscopy images at room temperature were acquired while cycling magnetic field between -8 mT and $+8$ mT, both in longitudinal and transversal mode. The particular benefit of this technique is that it allows one to locally map the IP magnetization of the MFC (in contrast to MOI and TMR which pick up the OOP component of the stray field). Thus, magnetic domains become visible and their evolution as a function of the applied IP field can be tracked. From the average intensity of these images over a chosen area it is also possible to reconstruct magnetic hysteresis loops. Figure 1(a) shows hysteresis loops obtained at different regions of the MFC labeled 1-6 in panel (c) for an IP magnetic field perpendicular to the gap. Panel (c) shows the longitudinal MOKE signal (Kerr sensitivity with respect to the vertical magnetization component) at $\mu_0 H = 1.1$ mT. The observed color contrast corresponds to variations of the vertical component of the local magnetic moment m_y thus revealing the magnetic domains. Note that in panel (a), saturation and coercivity are position dependent properties. This is more apparent in panel (b) showing the coercive field as a function of the labeled location indicated in panel (c). Note that a variation of $\mu_0 H_c$ as large as a factor of 2 can be obtained on the same device. An animation of the evolution of the IP magnetic domain distribution during the magnetization reversal process is shown in the Supplemental Material.

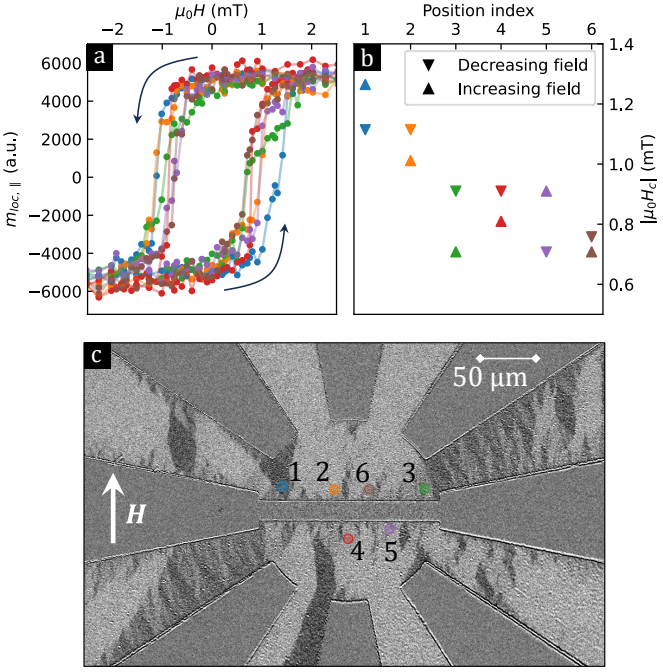

FIG. 1. (a) Hysteresis loops obtained by averaging the MOKE signal at the spots indicated in panel (c). The color code of the loops relates to the colors of the regions indicated in (c). The applied magnetic field is swept in the vertical direction, i.e. perpendicular to the gap. Measurements are acquired at room temperature. (b) Extracted coercive field as a function of the location of the spot indicated in (c). Panel (c) shows the longitudinal MOKE signal (Kerr axis vertical) at $\mu_0 H = 1.1$ mT. The observed color contrast corresponds to variations of the vertical magnetization m_y thus revealing the magnetic domains.

II. SCANNING TMR IMAGING

A. Experimental details

Hysteretic magnetization loops were acquired with a commercial TMR sensor fabricated by Micro Magnetics Inc. A 2×4 µm^2 elliptical junction has been patterned ~ 5 µm from the lapped corner of a Si substrate and the sensor exhibits approximately linear sensitivity to OOP stray magnetic fields from the sample ($\Delta V = 1.4654$ mV/mT with a 10 µA, 1.032 kHz drive current). To measure the magnetization, a 3-axis

piezoelectric stage was used to position the TMR sensor just above the center of the 20 μm slot at a point near the edge where the OOP component of the field was maximum. The IP magnetic field generated by a Helmholtz coil pair was then swept in a loop with extrema $\mu_0 H_{\rm IP} = \pm 2$ mT while the sensor voltage was recorded. During measurements the sample was mounted on the cold head of a low vibration commercial cryocooler inside an evacuated cryostat, allowing the temperature to be stabilized in the range 60-300 K.

B. Hysteretic response

Figure 2(a) presents hysteresis loops for different devices recorded using the TMR sensor at $T = 70$ K for IP magnetic fields between -2 mT and $+2$ mT. Note that the 2-petal device exhibits a lower coercive field than the 8-petal MFCs. No significant differences among the various 8-petal devices are observed, neither for those including YBCO petals nor for different gap sizes. Fig. 2(b) presents the hysteresis loops of the 8-petal devices for several temperatures. No detectable change is observed at the superconducting transition. The extracted saturation fields (i.e. the field B_z measured at -2 mT) and coercive fields for each temperature and device are compiled in Fig. 2(c) and (d), respectively. Panel (b) shows the measured OOP saturation field, $B_{\rm sat}$, at the edge of the gap as a function of sample temperature. This measurement should be a good proxy for the temperature-dependent saturation magnetization, $M_{\rm sat}$, near the center of the Py concentrator. Fig. 2(d) shows the temperature dependence of the measured IP coercive field, $\mu_0 H_c$. As temperature decreases, we observe a weak increase in both the saturation field (panel (c)) and the coercive field (panel (d)) consistent with previous reports on Py films[1,2]. Note, however, that there is no indication of a change in behavior of either parameter when the YBCO switches from being a non-magnetic metal at e.g., $T = 90$ K ($T > T_c = 87$ K) to a strongly diamagnetic superconductor at e.g., 60 K ($T < T_c$). In particular, the superconducting transition in the YBCO elements does not seem to induce an enhancement of the magnetic field concentration efficiency.

C. Mapping of the out-of-plane component of the stray field

Fig. 3 shows scanning TMR images of one quarter of the concentrator sample studied in Fig. 4. These images were captured using the 3-axis piezoelectric stage to raster scan the sensor across the surface of the sample to generate a 50×50 pixel map of the OOP field, B_z, at temperatures well below (60 K) and above (90 K) the superconducting T_c of the YBCO film. In each case the sample was cooled to the target temperature and an IP of $\mu_0 H = 2$ mT applied perpendicular to the 20 μm slot in the center of the concentrator prior to imaging. The TMR sensor was initially positioned about 25 μm above the sample surface to prevent any danger of making contact with it during these rather large area scans. Fig. 3(a,b) shows maps of the OOP magnetic field, B_z, above one quarter of an 8-petal Py/YBCO 'flower' structure at (a) 60 K and 90 K (b), well below and above the YBCO superconducting T_c, respectively. The measurement geometry shown in panel (d) indicates the position of the scanning area with respect to the MFC. Panel (c) shows the differential image (pixel-to-pixel numerical subtraction) between the magnetic maps above and below T_c. We found that when the YBCO petals are in the superconducting state, a slight narrowing and increase in amplitude of the main intensity peaks at the Py poles is observed, along with a weak suppression of the measured field at long distances. Therefore, the YBCO petals act to make the concentrator slightly more invisible at long distances outside its footprint.

III. SQUID MAGNETOMETRY ON PLAIN FILMS

The Py has been characterized on different substrates before and after patterning via SQUID magnetometry. In Fig 4, we show the results for Py films grown on different substrates. The permeability obtained for the 100 nm film on Si by fitting the maximum slope of the hysteresis loop is $\mu_{FM} = 2 \cdot 10^4$. This value is underestimated due to the minimum field-step imposed by the equipment. When using a LAO substrate, the permeability and the saturation magnetization are reduced whereas the coercivity increases. The figure also shows that the presence of YBCO droplets on the substrate increases the saturation field.

IV. SUPPLEMENTAL ANIMATIONS

A. Animation: MOI out-of-plane trapped magnetic field

The animation Tc-MOI.mp4 shows the MOI intensity map as a function of temperature of the trapped magnetic flux. The initial state was obtained by cooling down the sample to the base temperature of our cryostat (~ 4 K) while applying an OOP magnetic field $\mu_0 H_{FC} = 4$ mT, subsequently the field is turned off and the magnetic field landscape revealing the field-cooled trapped flux is monitored as a function of temperature.

B. Animation: Field dependent magnetic domain distribution obtained from MOKE microscopy

The animation MOKE.mp4 shows the MOKE intensity maps for transversal (left) and longitudinal (right) configurations as a function of the IP magnetic field applied vertically. Images were obtained with a 20x objective, the field of view corresponds to 552×345 μm^2. For each magnetic field, 8 images were averaged.

REFERENCES

[1] C. Luo, Y. Fu, D. Zhang, S. Yuan, Y. Zhai, S. Dong, and H. Zhai, "Temperature dependent coercivity and magnetization of light rare-earth nd doped

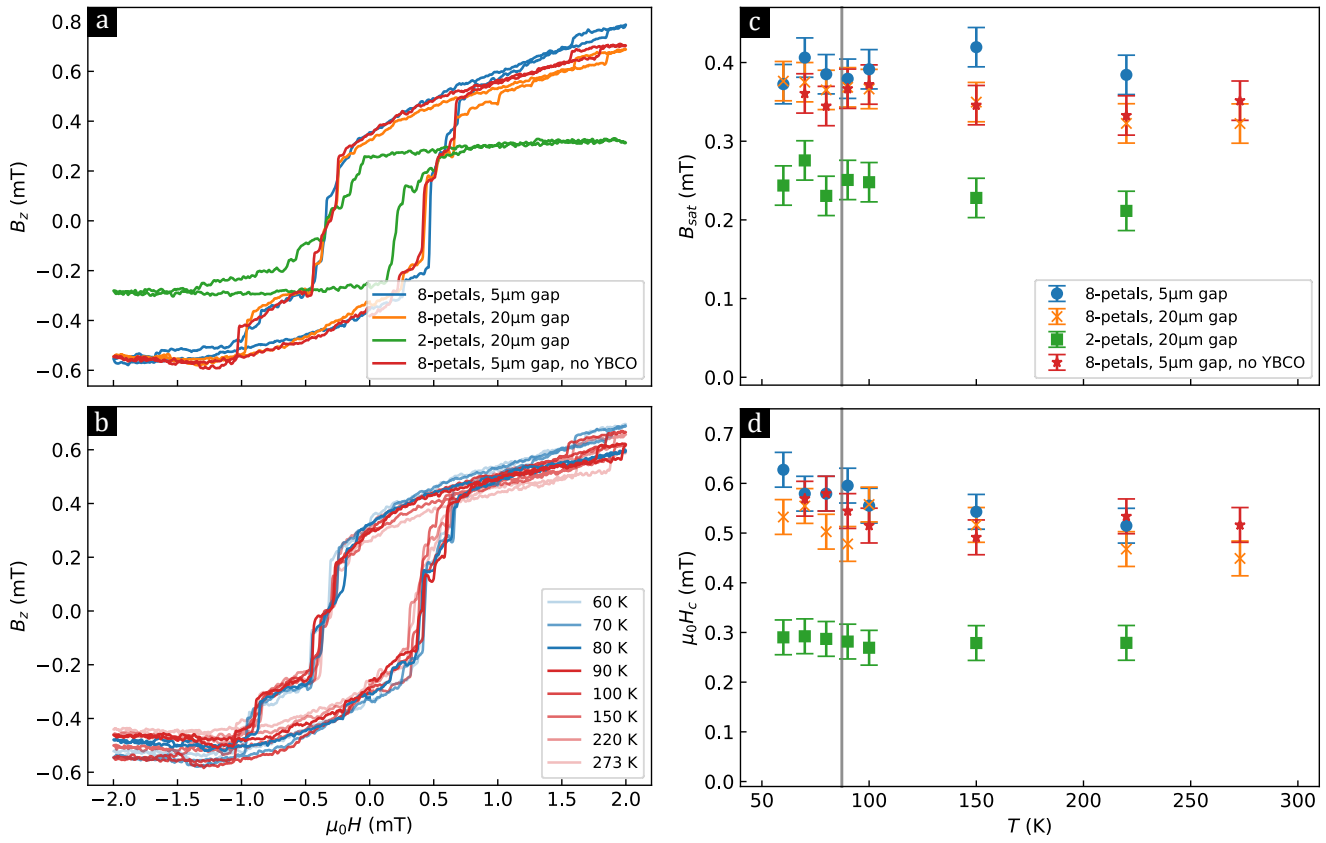

FIG. 2. (a) TMR sensor magnetic hysteresis loops for 4 different devices at $T = 70$ K. (b) Hysteresis loops for various temperatures for an 8-petal Py/YBCO concentrator structure with a 20-μm-wide slot. No detectable change is observable between data obtained below (blue) and above (red) the superconducting transition $T_c = 87$ K. (c) Saturation field and (d) coercive field as a function of temperature extracted from the hysteresis loops for various devices. The vertical gray line indicates the superconducting transition.

permalloy thin films," Journal of Magnetism and Magnetic Materials **374**, 711–715 (2015).

[2]Y. Zhao, Q. Song, S.-H. Yang, T. Su, W. Yuan, S. S. P. Parkin, J. Shi, and W. Han, "Experimental Investigation of Temperature-Dependent Gilbert Damping in Permalloy Thin Films," Scientific Reports **6**, 22890 (2016).

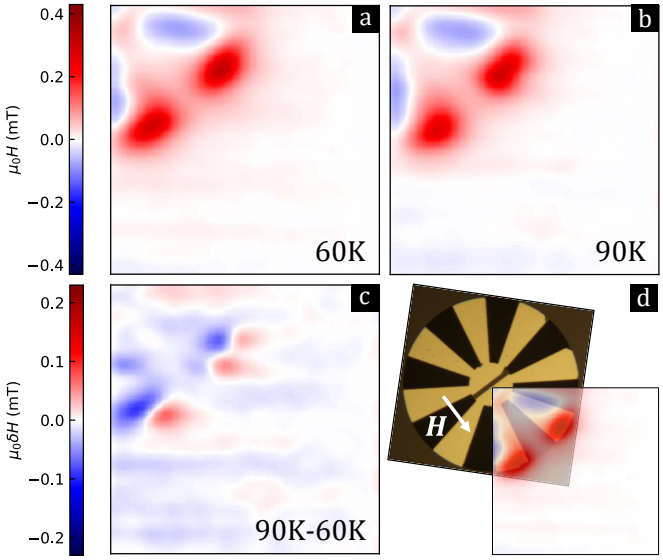

FIG. 3. Scanning TMR maps of the out-of-plane component of the magnetic field of an 8-petal Py/YBCO concentrator structure under an in-plane applied field of 2 mT applied perpendicular to the 20 µm-gap at (a) 60K $< T_c$ and (b) 90K $> T_c$. (c) Pixel-to-pixel numerical difference between the magnetic maps above and below T_c. (d) Overlap of the magnetic landscape on top of an optical image of the concentrator. The scanned area corresponds to a region of 750×750 µm^2.

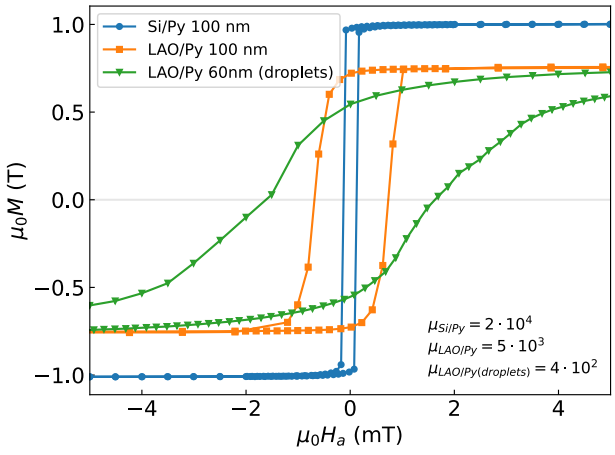

FIG. 4. Magnetization hysteresis curves obtained for Py deposited on Si, LAO and LAO presenting YBCO droplets. The saturation magnetization decreases with LAO substrate whereas the coercive field increases.